VILNIUS UNIVERSITY
FACULTY OF PHYSICS
INSTITUTE OF PHOTONICS AND NANOTECHNOLOGY

Gytis Babaitis

STUDIES OF PHOTOLUMINESCENCE INTENSITY AND PEAK WAVELENGTH CORRELATION IN POLAR AND NON-POLAR InGaN MULTIPLE QUANTUM WELLS

BACHELOR THESIS

Light Engineering study program

Student	Gytis Babaitis
Supervisor	dr. Darius Dobrovolskas
Institute representative	dr. Steponas Raišys

Vilnius 2023

Table of Contents

Introduction 3
Indium Gallium Nitride 4
History and Definition 4
Growth 5
C-plane Samples and Internal Electric Field 7
M-plane Samples 8
Multifunctional Microscope System Alpha 300 10
Principles of Confocal Microscopy 10
Components 11
Experimental Setup 13
Results & Discussion 15
C-plane – PL spatial distribution 15
Localization 16
Spectral Characteristics 17
Correlation 19
M-plane Results 23
M-plane Set Correlation 25
Conclusions 27
Santrauka 29
References 30

Introduction

Over the last three decades research on InGaN, has opened new possibilities and revolutionized the LED and even general lighting industries. Publications by S. Nakamura on InGaN/GaN double heterostructures [1] and achievements in p-doping in GaN by I. Akasaki and H. Amano [2] lead to massive improvements of the technology. This is supported by the Nobel Prize committee as in 2014 the three scholars (S. Nakamura, I. Akasaki and H. Amano) that kickstarted the field back in the 1990s were awarded the Nobel Prize in physics, as stated by The Royal Swedish Academy of Sciences: *"for the invention of efficient blue light-emitting diodes which has enabled bright and energy-saving white light sources"* [3]. Due to the use of these LEDs, there were immense energy savings in the world, as a quarter of the energy used on Earth is for lighting. The extremely high efficiency of InGaN/GaN QW structure devices solidified their place in solid state lighting and are still at the top for blue LEDs. Microcavity lasers and high-efficiency LEDs can also be manufactured with InGaN and GaNAs [4]. Along side manufacturing of LEDs and laser diodes (LDs), InGaN is being used in the photovoltaic industry [5]. The advantage of bandgap engineering from ~ 0.7 to 3.4 eV, which also covers almost the entire solar spectrum is relevant for solar cell efficiency improvements. Modeling shows that by using multi-junction design and InGaN as the material, efficiencies over 50 % could be achieived [6]. Moreover due to the electric conductivity of InGaN and piezoelectric effect present in the material, it can be used for harvesting and converting electrical, solar and mechanical energy. Piezotronics/piezo-phototronics and piezoelcetrochemical (PEC) hydrogen generation devices have been studied [7]. However, the same piezoelectric field causes QCSE and efficiency droop at longer emission wavelengths. The purpose of this bachelor work was to analyze correlation coefficient between photoluminescence peak emission wavelength and photoluminescence intensity of indium gallium nitride (InGaN) grown on both c-plane and m-plane surfaces, analyze observed patterns and get a deeper understanding on the physical phenomenon behind InGaN/GaN light emitting diodes that may hamper its efficiency and industrial applications. Whilst the work tasks were to:

1. Analyze scientific publications on InGaN/GaN multiple quantum well samples, growth of both c-plane and m-plane, material problems and commercial applications.
2. Measure spatial photoluminescence distributions of c and m-plane InGaN/GaN MQW samples using a confocal microscopy setup.
3. Analyze, discuss and explain the measured results.

4. Formulate conclusions explaining the obtained results.

Indium Gallium Nitride

History and Definition

Indium gallium nitride (InGaN) is classified as a ternary compound in the III-V semiconductor group as it is made up of three materials, of which the first two (indium, gallium) are in the third group in the periodic table of elements and the last one (nitrogen) in the fifth, hence the name. InGaN light emitting diodes (LEDs) have been of interest to the scientific community for the possibility to produce devices emitting through the whole visible range with a single alloy. This could be done by varying the amount of indium (In) present in the material. The bandgap of pure InN is around 0.69 eV (~1797 nm) whilst that of GaN is around 3.4 eV (~365 nm) [8].

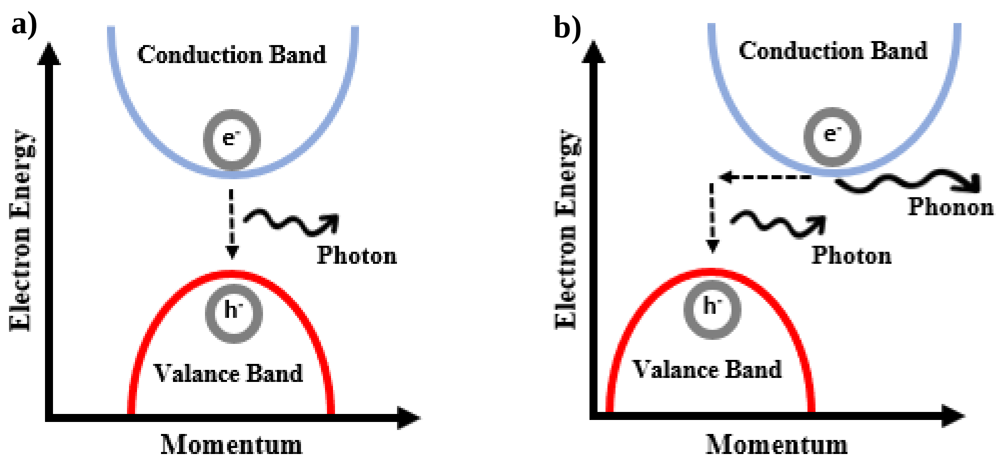

Fig. 1 Schematic representation of a) direct and b) indirect band gap semiconductors.

Semiconductors can fall within two groups depending on their band structure: indirect and direct bandgap. In indirect bandgap semiconductors the conduction band minimum and the valance band maximum are offset, and since a photon has almost zero momentum, conservation of momentum would not happen, and radiative recombination couldn't take place. However, it can be seen that an additional particle, a phonon is formed, which equalizes the difference between electron and hole momentums (Fig. 1 b). For InGaN everything is much simpler, as it is a direct bandgap material, in which holes in the valance band maximum and electrons in the conduction band minimum have the same momentum, it is conserved upon recombination and the probability of radiative jump from band to band is high (Fig. 1 a). This explains the huge differences when comparing external quantum efficiencies (EQE) of these two different band structure materials. The EQE of any LED could be expressed as the ratio of the number of emitted photons to the incident on the surface photons (in case of photoluminescence) or injected carriers (in case of electroluminescence). Typical indirect bandgap semiconductor such as Si LED has a EQE of around 0.02 % [9]. For InGaN/GaN devices emitting in the visible range and more precicly in the blue region, EQE even up to 80 % have been achieved [10]. However this is quite surprising when considering the amount of dislocations present with in this material, which reached up to 10^{10} cm^{-3} in early devices [11]. What is even more spactacular, dislocation densities six orders of magnitude smaller than that, in such devices as GaAs, would lead to nonradiative recombination, then overheating of the device and finally terminal damage [12]. This shows how robust InGaN can be against extended defects.

In this work multiple quantum well (MQW) samples were measured. This heterostructure is used in LEDs in order to increase the efficiency. MQW is a part of semiconductor device that consists of a stack of thin layers of semiconductor material separated by very thin layers of a different material where electrons and holes are confined so tightly that their wavefunctions overlap, increasing the probability of radiative recombination. The thickness of the active region is determined by the deBroglie wavelength of the materials electron [9]. This wavelength is inversly proportional to the momentum of the particle (p), and is calculated with the following formula [13]:

$$\lambda_{dB} = \frac{h}{p} \tag{1}$$

where h is the Planck constant.

Growth

Growth of InGaN samples still remains as one of the key hurdles to overcome in the field. Scientists are hard at work trying to improve the quality of grown samples. The main issues facing them is: a) equilibrium vapor pressure (EVP) differences between InN and GaN [14] and b) large lattice mismatch between InN and GaN (~ 11 %), as well as high lattice mismatch between InGaN and the substrate itself [12], [15], [16]. To grow high quality materials it is crucial to precisely control such parameters as V/III reactant source precursor ratios, growth pressure and temperature. Studies on improving for example V/III ratios through the transition of growth mechanism are have been worked on [17]. Two most often used growth techniques are: molecular beam epitaxy (MBE) and metalorganic chemical vapor deposition (MOCVD). MBE is a thin single crystal layer deposition technique which uses molecular beams that are generated in Knudsen cells. The growth takes place in an ultra-high vacuum (UHV) chamber. The source beams can be generated in numerous ways: a) ion beam bombardment, b) melting and evaporation of various solids or liquids contained in crucibles, c) solid sublimation from a crucible, etc. [18] The UHV employed in this technique features very low partial pressures (typically around $< 10^{-14}$ Torr), which leads to very low background impurity levels [19]. Usually MBE has slow deposition rates of around 50 nm/h [9]. Higher rates can be achieved but then ion damage can be observed. However one of the advantages of MBE is low substrate temperature (around 500 ^oC) leading to minimal material and dopant interdiffusion, lower stress upon cooling and reduced alloy segregation [20].

The other, maybe even more popular growth technique – MOCVD, is a non-equilibrium growth technique, where growth of materials is by relying on vapor transport of the precursors and chemical reactions, instead of physical deposition as in MBE. Furthermore, opposite to MBE for the reactions in the MOCVD chamber to take place and to crack the ammonia molecules temperature has to be high (> 1000 ^oC). These reactors have to overcome temperature, precursors flow and film uniformity problems. There are many designs of reactors, including vertical and horizontal flow, atmospheric and low-pressure reactors. When considering pressure, atmospheric reactors are favored because it is possible to achieve high partial pressures of ammonia. [9]

Besides the growth technique and parameters, substrates also make difference in the quality of the sample. Typically, InGaN/GaN MQWs are grown on a sapphire (Al_2O_3) substrate. However, as mentioned above, large lattice mismatch is a problem which can lead to high number of threading dislocations as well as deterioration of surface morphology and drop in device performance. Semi-bulk approach has been researched [21]. By slowly increasing the GaN thickness whilst the growth of the semi-bulk continues, researchers were able to achieve defect densities comparable with bulk GaN. This is due to the ability of semi-bulk to relax through V-pit formation whilst grown, because GaN provides a back filling mechanism. Such growth technique is also compatible with MOCVD growth.

C-plane Samples and Internal Electric Field

Group III nitrides can have either a zinc blende or wurtzite structures. For both cases III group atoms are surrounded by four nitrogen atoms and each such atom is surrounded by four III group material atoms. These structures mainly differ in the stacking sequence and the wurtzite has been known to be more thermodynamically stable and quite easy to grow. [22]

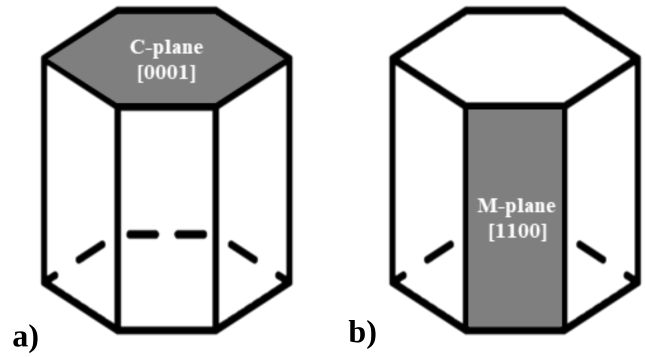

Fig. 2 Schematic view of a) the polar [0001] c-plane and b) non-polar [1100] m-plane within the hexagonal wurtzite structure

Wurtzite structures have hexagonal symmetry. There are planes on which you could grow your material. The ones that are the most relevant for this work are c-plane (Fig. 2 a) and m-plane (Fig. 2 b). Most of the research and progress concerning InGaN devices has been on the polar c-plane orientation as high quality GaN substrates are available [23]. Although the availability and the quality of c-plane samples is good, the downside of using this orientation is that due to lattice mismatch, biaxially compressive strain induces piezoelectric polarization. When growing QWs the strain changes the quantum confined sub-bands and leads to piezoelectric field along the z plane in wurtzite materials. This internal electric field (IEF) separates holes and electron towards the different sides of the well due to opposite charges (Fig. 3 b). Therefore, the presence of such field has a profound effect on optical properties [9], [24]. It tilts the energy bands of InGaN and reduction in internal quantum efficiency (IQE – expressed as the number of charge carriers or electron-hole pairs generated to the photons absorbed) can be observed. This is known as the quantum confined Stark effect (QCSE) [25]. Along with the decrease in radiative recombination, other adverse effects include red-shift of emission peak position and widened spectra at full width-half maximum (FWHM) [26]. The peak position shift is interconnected with In amount in the grown material, as higher amounts of indium increases the piezoelectric field, which induces the QCSE [17]. One of the biggest problems still facing InGaN LEDs is efficiency drop at longer peak wavelength devices, which also is known to be influenced by the piezoelectric field [27]. Hole injection into the QW becomes less efficient and electron leakage from the QW increases with increasing IEF.

Clearly the IEF is something scientists want to avoid. One of the compensation methods is the so called "piezo-phototronic" effect. It alters the built-in electric field with external stress. Then new polarization charges are created that compensate the original ones. This means the InGaN energy bands tend to flatten out, which increases the electron-hole wavefunction overlap and radiative recombination in the process. However, precision in this method is key, because if the applied stress is increased further, polarization charges tilt the energy bands in the opposite direction, and same negative effects are observed.

Furthermore, as mentioned before the substrate choice plays a crucial role in achieving high quality structures and materials. It can also affect the IEF. Studies on replacing the typical sapphire substrate, with silicon have been reported . Electron and hole distribution in the MQWs seems to be more inhomogeneous on sapphire than that on silicon [27]. This inhomogeneity leads to increased Auger recombination rate and poor efficiency of devices. Using silicon as the substrate reduced the IEF in the MQWs by around 40 %, compared to sapphire. Use of silicon as a substrate also is attractive for industrial purposes, as the cost of the devices would be significantly reduced.

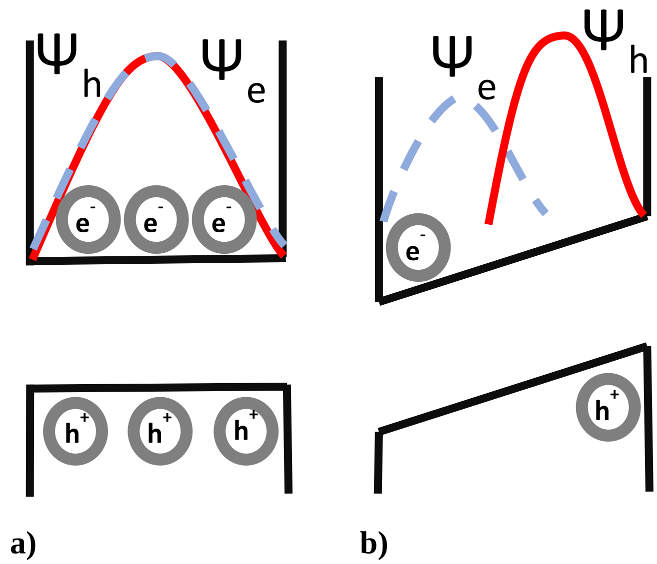

Fig. 3 Band profiles of quantum well without a) and with b) the effect of piezoelectric field in InGaN.

M-plane Samples

To avoid the piezoelectric effect, it is possible to use nonpolar planes such as a-plane and m-plane, which due to their crystal symmetry have no spontaneous polarization. The first nonpolar m-plane samples that were grown on $LiAlO_2$ substrates, by P. Waltereit and his team were published about back in 2000 [28]. Although the quality of the samples was significantly worse than its c-plane counterparts, it was nevertheless good enough to show that indeed m-plane grown crystals were free of any polarization field. When QWs are grown on these planes the energy bands remain flat, and the wavefunction overlap is not affected [29]. It would seem logical to grow samples using these orientations, however there are issues.

Main drawback is the quality of such samples. Indium incorporation is heavily affected by crystal growth orientation. In incorporation efficiency has been compared between polar, semipolar and nonpolar InGaN layers [30]. The results showed that poorest indium incorporation was with nonpolar orientation, followed by semipolar and polar. For the same respective orientation indium content was 6.4, 6.9 and 21.3 %, when growth conditions were equal. This shows that it is difficult to get high indium incorporation with other than c-plane orientations. This then defeats the main advantage of InGaN which is the broad bandgap tunability due to different indium incorporation. Another m-plane growth issue is the adatom mobility difference, which leads to different growth dynamics and consequently different growth conditions. On top of that anisotropic lattice mismatch is present in m-plane InGaN, which could lead to extended defects and finally even macroscopic cracks along the material surface [31].

Furthoremore, although theoretically nonpolar LED devices should be more efficient D. Sutherland *et al.* have shown that m-plane InGaN/GaN MQWs grown using before mentioned MOCVD technique, exhibit lower quantum efficiencies. This observation is not fully understood but could be attributed to the defects caused by difficulties in sample growth. [32]

With that said, there is of course pros to this orientation that makes it such a hot topic for researchers. Mainly pros stem from the fact that there is no, or little electric field within in the device. The IQE of polar QWs, emitting at green wavelengths is much lower than for the nonpolar counterparts. As those devices need to have more In larger strains become inevitable. This means longer radiative lifetimes, that increases the probability to reach nonradiative recombination centers (NRC's), that manifests itself as lower IQE values [33]. Lack of IEF also means that the design of the device can be simpler, decreased electronic wavefunction distortions and increase in the accessible spectral range could be achieved. Hence further research and advances in this field could help reach even more efficient solid state lighting solutions.

Although there is a big advantage in the lack of IEF, nonpolar samples still are extremely difficult to grow and have their own inherent problems. This along with cost and other drawbacks means that there is a limited bank of knowledge for m-plane InGaN.

Multifunctional Microscope System Alpha 300

Principles of Confocal Microscopy

The first ever confocal microscopy system was introduced by Marvin Minsky back in the mid-1950s and shortly after patented in 1957 [34]. The basic idea of confocal microscopy is simple yet ingenious. It works by employing a point light source which is focused on to the sample by a lens (or lens system). However, if the sample has some thickness, it will luminesce not only from the point which is in the focal plane of the lens. In a conventional widefield optical microscope you would collect these out of focus rays, which would contribute to some background haze in the image. Confocal microscopy overcomes this issue with a very simple, yet elegant solution – a pinhole. This pinhole rejects the out-of-focus light rays, that would otherwise worsen the resultant image. As the pinhole is placed at exactly the position where the focal point of the lens should produce the image, these two points are known as "conjugate points". The pinhole is **conjugate** to the **focal** point of the lens, thus it is a **confocal** pinhole, hence the name of the microscopy setup.

The point light source is then scanned through the sample (either by moving the light beam or the sample itself), so for this system there is never a complete image at any given point. The measured light from one point is collected by a detector and with the help of a connected computer a whole image can be built up.

As only a small fraction of the out of focus light passes through the pinhole, the resolution is enhanced, compared to conventional microscopy techniques. With that said confocal microscopy is still nowhere near the capabilities of such techniques as transmission electron microscopy (TEM).

Confocal microscopy most often uses visible light. The resolution of this (as well as conventional techniques) is limited by the employed excitation light wavelength and is described by the Abbe theory in 1873 [35]. He stated that the object in image space is resolved if at least the first diffracted order of an object is captured by the lens system. Another important criterion for resolution is the Rayleigh criterion, which states that we are still able to resolve two objects if the first Airy pattern is at the first minimum of the second.

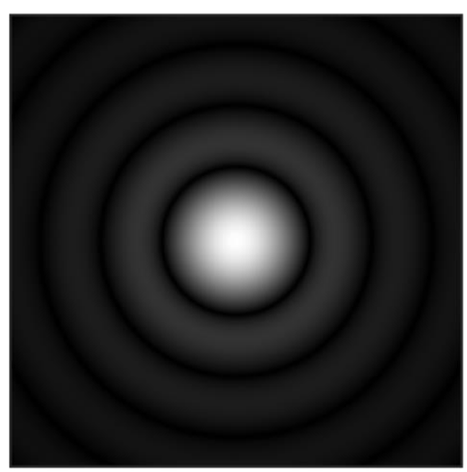

Fig. 4 A computer-generated image of an Airy disk.

The Airy pattern is depicted in Fig. 4 [36]. In a perfect lens system, that has a circular aperture, the point image should be such a pattern. 84 % of light is collected within the central bright spot and 91 % within the second dark ring. The Rayleigh criterion can be written mathematically for a circular aperture as [36]:

$$\Delta x = 0.61 \cdot \frac{\lambda}{NA} \tag{2}$$

where λ is the excitation light wavelength and *NA* is the numerical aperture of the used lens system. *NA* is simply the maximum light acceptance half-angle (α) of the lens system, its formula is:

$$NA = n \cdot sin\alpha \tag{3}$$

here n is the refractive index of the medium between the lens and object.

Components

The scheme of the system used for experiments is shown in Fig. 5. As confocal microscopy requires a point light source, in this setup it is a LD. The beam is transmitted via a single mode optical fiber (*C12.1*). This type of fiber transmits only a single transversal mode (Gaussian beam). A coupling unit (*C6*) connects the fiber with the microscope. Once inside the microscope a dichroic mirror (*C4*) guides the beam through the objective (*C3*) and is then focused onto the sample. After the sample emits a luminescence signal, it is collected by the same objective and is directed as a parallel beam toward the top of the microscope (*C10*). In the middle of the signal path the system is fitted with a filter (*C7*) which cuts out the laser diode beam signal, that might interfere with the luminescence signal. The light from the sample is directed through another optical fiber (*C12.2*). The core of this multi-mode optical fiber acts as the before mentioned pinhole. The optical fiber is connected to a spectrometer and the final spectrum is registered by a thermoelectrically cooled (to -68 ^{o}C) charge-coupled device (CCD) camera. The laser is raster-scanned across the sample by scanning in all axes and the image is acquired line by line. Finally, the acquired data matrix is written to a connected computer.

In the present microscope system, scanning of the beam is done by moving the sample itself. A piezoelectric scan stage (*C2*) is used for this purpose. Its closed loop resolution is ≤ 1 nm for X and Y axis (side-to-side), and ≤ 0.1 nm for Z axis (*C15*) (up and down). The objective turret (*C3*) can hold up to five objectives. For our measurements a high aperture (NA = 0.9) *Nikon* objective with a magnification of 100, and a working distance of 0.26 mm was used. The system also has a beam deflection unit (*C5*), for AFM and SNOM modes to detect the bending of the cantilever during the measurements.

The LD operating in continuous wave (CW) regime had an excitation wavelength of 405 nm. In order to modulate the excitation intensity throughout the measurements a round continuously variable metallic neutral density filter (*C16*) was used.

The microscope itself is controlled via software provided by the manufacturer. After the measurements, data is analysed partially by the aforementioned software and with *OriginLab* program.

C1 – XY positioner

C2 – Scan stage

C3 – Objective turret with objectives

C4 – Dichroic mirror

C5 – Beam deflection unit

C6 – Laser coupling unit optical output

C7 – Filter slider unit

C8 – Binocular tube with ocular camera

C9 – Filter holder for reflection mode measurements

C10 – Fiber coupling unit optical output

C11 - Pushrod

C12.1 – Laser diode optical fiber

C12.2 – CCD camera optical fiber

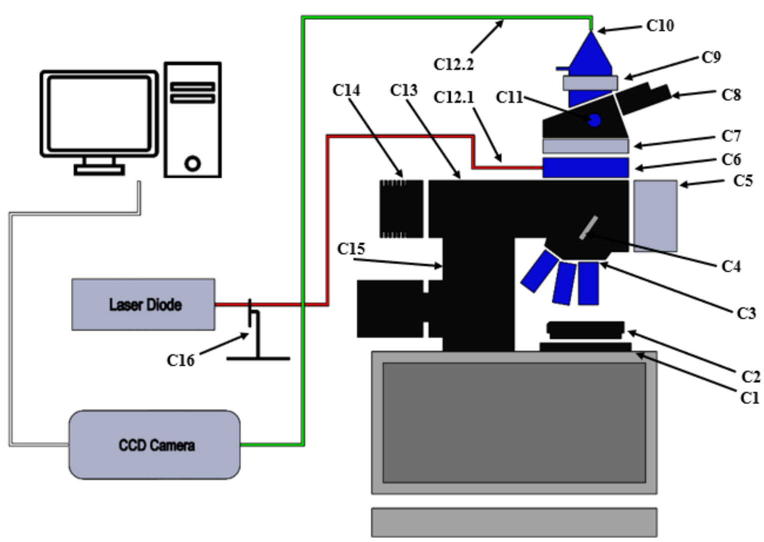

Fig. 5 Scheme of confocal microscopy system with numbered components.

C13 – Microscope body with Köhler illumination

C14 – Light source

C15 – Microscope Z stage stepper motor

C16 – Round continuously variable metallic neutral density filter

Experimental Setup

In the present work InGaN/GaN MQWs grown both in c-plane and m-plane orientations were studied. Because of the relatively optimized growth procedure, the c-plane samples usually are of higher quality even for high indium content. They cover a wide spectral range from around 420 to 660 nm. Compared with c-plane samples, the growth of m-plane samples is more difficult and makes it prone to defects and dislocations. In this study m-plane samples have lower indium content and thus luminesce in the blue region of the visible light spectrum. The samples are divided into four sets and are sorted according to the amount of indium, with the first sample having the smallest amount (in the case were In is equal the order is determined by the width of the QW). The first three sets incorporate the c-plane samples, whilst the fourth set is of m-plane samples. Indium content along with QW width for all samples is depicted in the Table 1. All of the samples were grown by MOCVD technique. Prof. Jim Speck's team from the University of Santa Barbara California was responsible for the growth of three of the four sample sets (1^{st}, 2^{nd} and 4^{th}), whilst the 3^{rd} set was grown here in Vilnius, Lithuania at the Institute of Photonics and Nanotechnology and supervised by dr. Arūnas Kadys.

Table 1 Detailed sample structure parameters

Set	**1^{st}**			**2^{nd}**			**3^{rd}**				**4^{th}**					
Orientation	*C-plane*										*M-plane*					
Sample No.	S1- 1	S1- 2	S1- 3	S2- 1	S2- 2	S2- 3	S3- 1	S3- 2	S3- 3	S3- 4	S4- 1	S4- 2	S4- 3	S4- 4	S4- 5	S4- 6
Indium amount (%)	~ 25	~ 25	~ 25	~ 12	~ 17	~ 20	~ 20	~ 22	~ 25	~ 25	~ 10	~ 13	~ 13	~ 13	~ 14	~ 14
QW width (nm)	~ 2	~ 2.7	~ 4	~ 3	~ 3	~ 3	~ 3.5	~ 3	~ 3	~ 4	~ 8	~ 7	~ 8	~ 8	~ 4	~ 4

The setup of the microscope system for measurements follows the description in the previous chapter. As additional investigation on carrier dynamics was conducted, it was crucial to know intensity of the excitation light upon the surface of the sample, so at the start of the measurements a calibration scale was determined by measuring the LD intensity before coupling to the optical fiber (*C12.1*) and after the objective in the place where the sample would be. In such way, by changing the intensity with the continuously variable metallic neutral density filter and placing the measurement instrument after it, the exact intensity would be known without the need to reset the samples position, as that would skew the results.

Five values of excitation intensity were chosen (1, 3, 9, 28 and 90 μW). 10x10 μm^2 (100×100 points) areas on the samples were chosen and the photoluminescence (PL) distributions were measured for each of the excitation conditions. Some samples had very high luminescence signal at higher excitation values, and it was saturating the detector, thus a neutral glass filter was implemented to lower the intensity without affecting the spectral characteristics of the measurement. When analyzing the results, the intensity was corrected by the use of *WITec 5.0* software supplied by the microscopy system manufacturer and *OriginLab* program. From the PL distribution images background was subtracted and Gaussian filter was fitted to extract such parameters as FWHM, peak position and intensity. The Gaussian filter was implemented in order to lower the possible errors of PL peak position detection. Erroneous values may be detected due to random noise in the system. These artifacts could skew the correlation calculations. The filter makes the spectrum smoother and more representative.

After all of the data was collected it was possible to calculate the correlation coefficient. As mentioned previously each of the images consisted of 10 000 points which meant the whole image could be represented as the same size matrix (100×100). Calculations with such large files (bearing in mind the number of samples and different parameters inside each one) would be very time consuming. For that reason, a code was written by me using MATLAB to automate the calculation procedure. To quickly and simply explain the working principle behind the code: first different parameter files of a single sample measurements are uploaded into MATLAB's workspace and then grouped according to the file names, which would correspond to certain excitation intensity. Then all possible combination pairs are made. Each of the matrix is converted into a column vector and after the outlier values have been removed the correlation could be found. After that the code also calculates statistics, such as average intensity, peak position and so on, along with their standard deviations. The code is run for each sample and all of the values are written onto an Excel spreadsheet.

Another program was used to help find the approximate internal electric field values for c-plane samples. The program works by solving the stationary Schrödinger equation and the Poisson equation. It then outputs the PL band peak position dependence on carrier density. The program was written by V. Liuolia and was previously used to calculate the IEF for AlGaN samples [37].

Results & Discussion

C-plane – PL spatial distribution

Highly inhomogeneous PL intensity was observed from the PL spatial distribution images of c-plane samples. Later acquired *Gauss center* images showed similar inhomogeneities with in

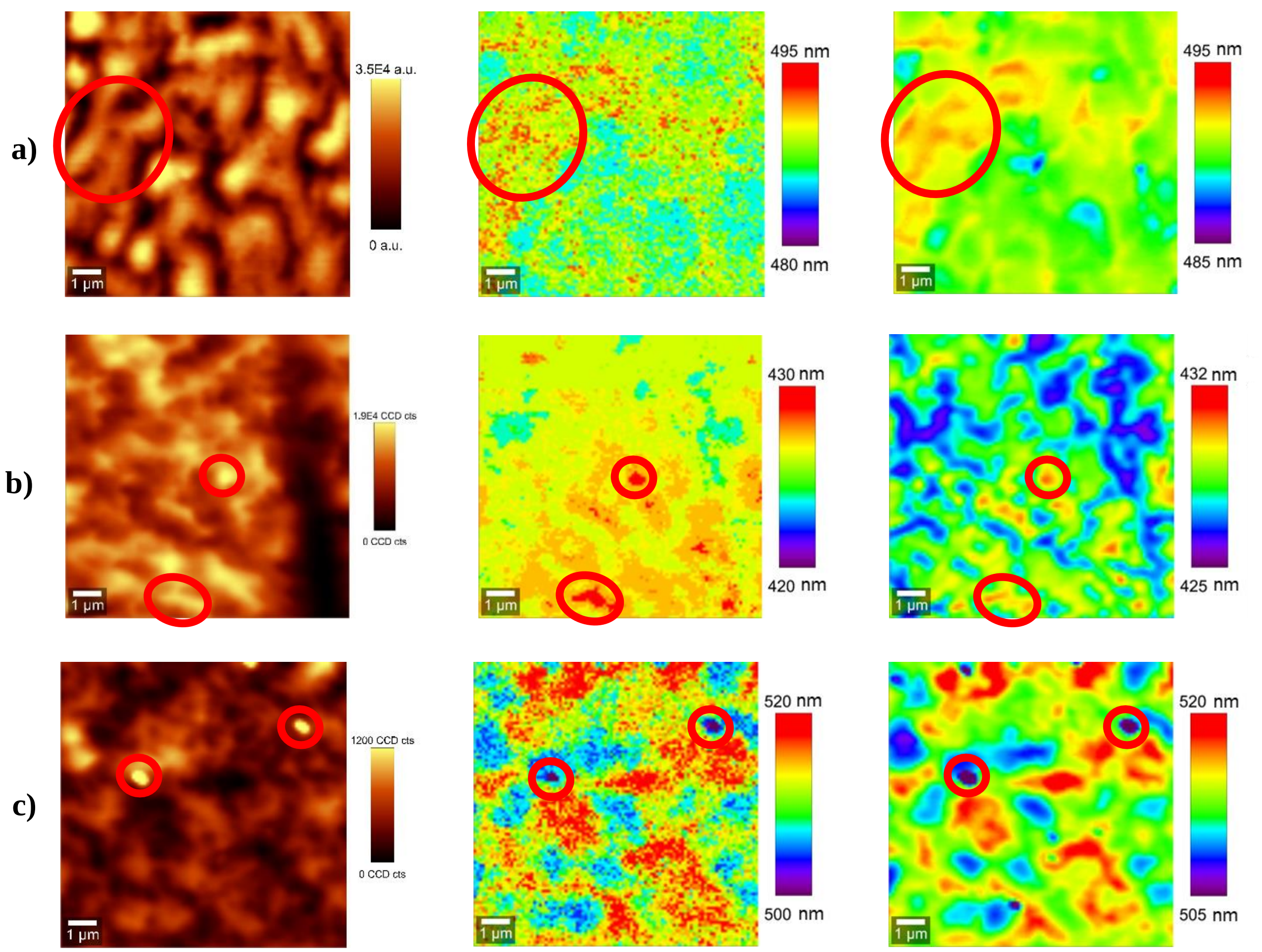

Fig. 6 Spatial distribution of spectrally integrated PL intensity, emission band peak position and Gauss Center of samples a) S1 – 1, b) S2 – 1 and c) S3 – 4 at an excitation intensity of 9 μW

the emitted wavelengths which was also confirmed with *Position of Maximum* data. This could be attributed to inhomogeneous distribution of indium. Fig. 6 depicts three samples that have shown the most distinct features observed in this sample series. Growth of InGaN even in c-plane orientation is still difficult for higher indium concentrations and this has been known to lower surface quality along with the increased formation of In-rich clusters [38], [39]. Images Fig. 6 c) depicts sample with one of the highest indium concentrations and a clear redshift of emission wavelength compared with samples in a) and b) can be observed. To see the statistical dependencies of the samples more clearly, spatially-averaged PL intensity and peak position values have been graphically represented in Fig. 7. The tendency of redshift emission wavelength was not as obvious to notice in the 3rd set as its samples had similar structure parameters. The overall peak position redshift is simply explained by the alteration of materials bandgap, as increasing In content lowers the bandgap energy, thus emission at longer wavelengths is observed. It has been noticed in numerous works as well [38], [40].

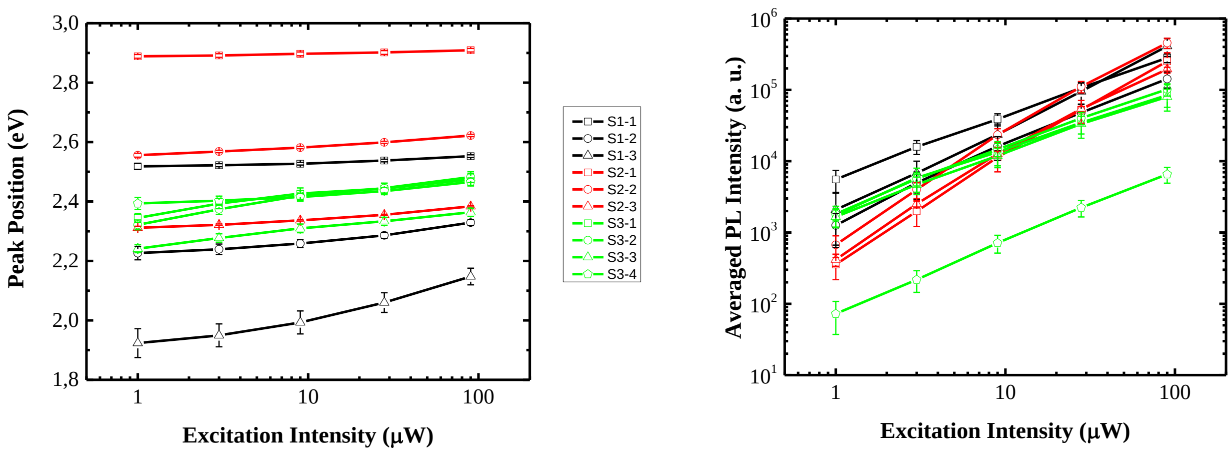

Fig. 7 Peak position and averaged PL intensity dependance on excitation intensity of 1st, 2nd, and 3rd sample sets [Error bars depict standard deviation for each value]

Localization

Fig. 8 depicts histograms for peak emission wavelength fitted with the gaussian filter (Gauss Center) sample S2-1, containing low amount of In, and S3-4 having one of the highest In percentages from all the samples. When looking at the histograms for both samples a clear widening can be observed, growing from ~ 13 meV for S2-1 to ~ 40 meV for S3-4. It indicates an increase in spatial inhomogeneity of In, with increasing In amount, which could be due to composition fluctuations or phase segregation when growing InGaN MQWs. As explained previously increasing In causes disorderly growth, which could increase NRCs. Partially relaxed areas could lead to higher densities of both defects and localized states, causing a broadening of the FWHM [41].

Furthermore, analysis with the Gaussian filter allowed to acquire FWHM values of the emission spectra. And although visually it is quite difficult to see, higher excitation intensities cause the spectra to narrow. FWHM values of S2-1 decreased from 106 meV to 88 meV, for lowest and highest intensities respectively. Same was true for S3-4 as emission spectra narrowed by ~ 11 meV (from 252 to 263 meV). Similar results have been reported by X. Wang *et al.* [38] and could be attributed to carrier redistribution to shallower localization states from deeper ones as well as screening of QCSE which will be covered at higher detail in later chapters.

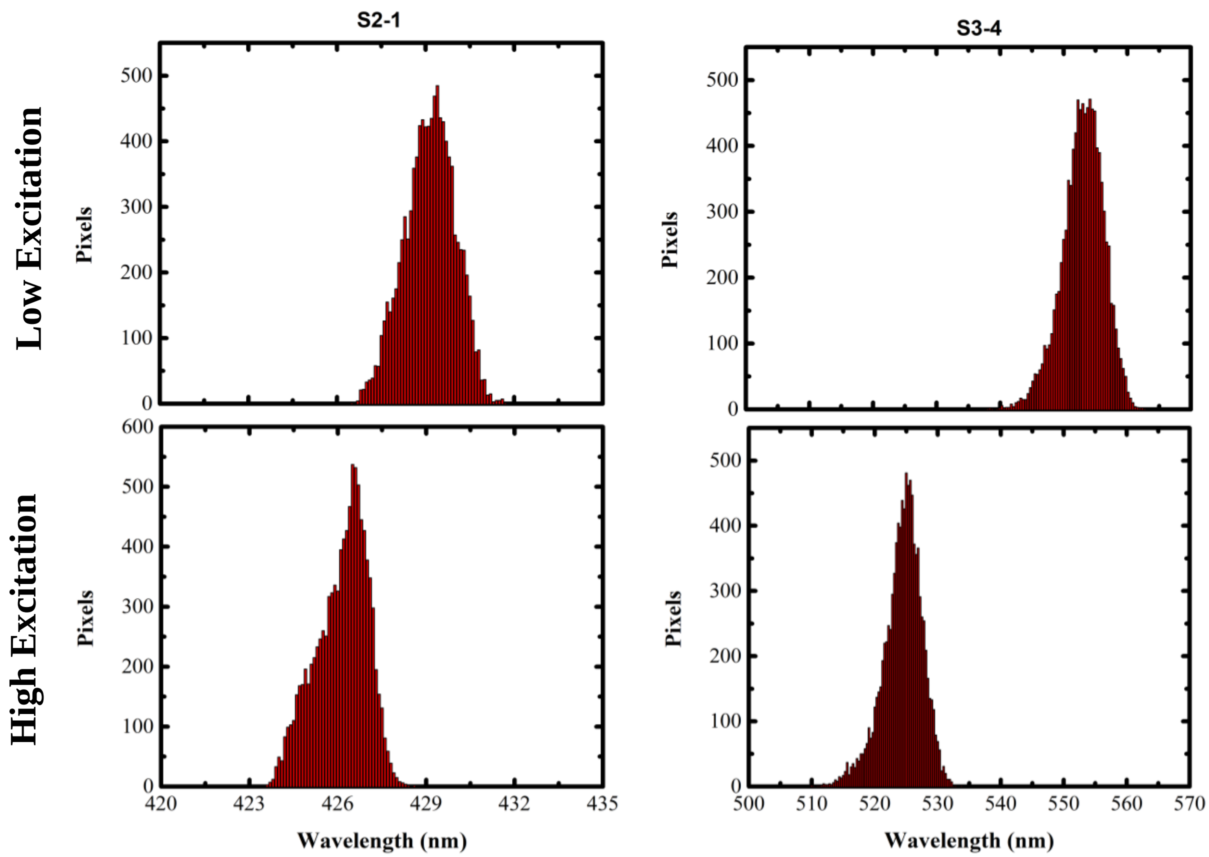

Fig. 8 Histograms of Gauss Center for samples S2-1 and S3-4 at lowest and highest excitation intensities

Spectral Characteristics

In Fig. 9 averaged PL spectrum of two samples emitting in the blue and amber-green regions of the visible spectrum can be seen. From both Fig. 9 and Fig. 7 it is visible that increasing the excitation light intensity causes a blueshift of emission wavelength. The emission bands ten to shift to shorter wavelengths or higher photon energies. This is typical for such materials and has been noticed in many works [38], [40],[42]. As the excitation is increased, density of photoinduced nonequilibrium carriers becomes larger and they are able to compensate for the present IEF with in the QW. When we increase the excitation even more the blue-shift tends to be due to band-filling effects [38]. Due to this effect electrons and holes fill bands from the bottom, and because the higher energy states are more dense, more carriers jump to those states and peak emission wavelength becomes shorter [40]. This is valid in the present samples as well, because samples with higher In content have stronger blueshift of emission, as those samples theoretically have higher IEF, its compensation is more pronounced.

Furthermore, both figures show that higher In percentage samples have lower averaged PL intensity, which also what was observed from the PL spatial distribution images in Fig. 6. This could be explained by poor growth for the samples containing higher In, which leads to more NRCs, as a consequence of increased dislocations.

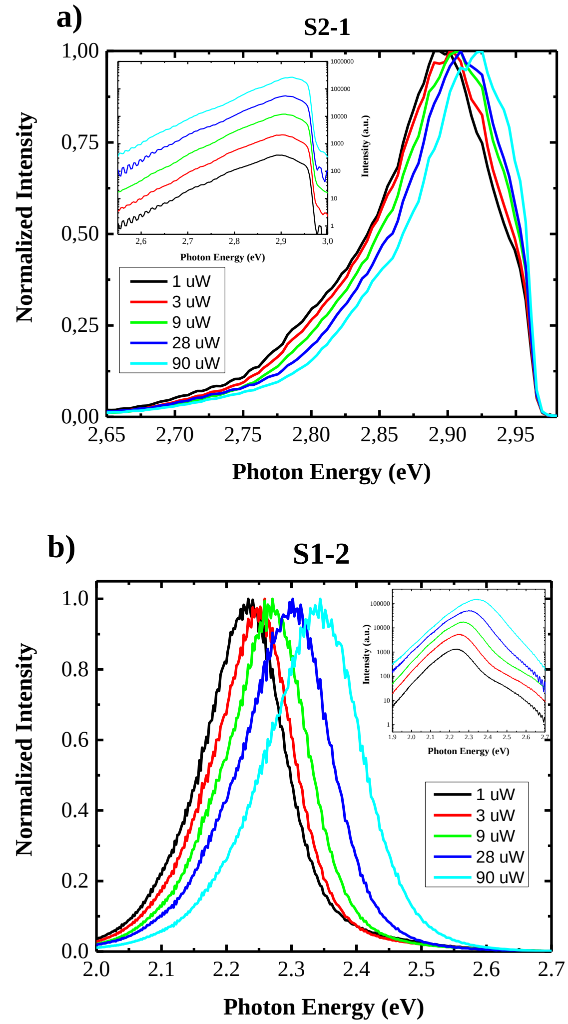

Fig. 9 Average PL spectra of samples emitting at a) blue and b) amber-green part of the visible spectrum.

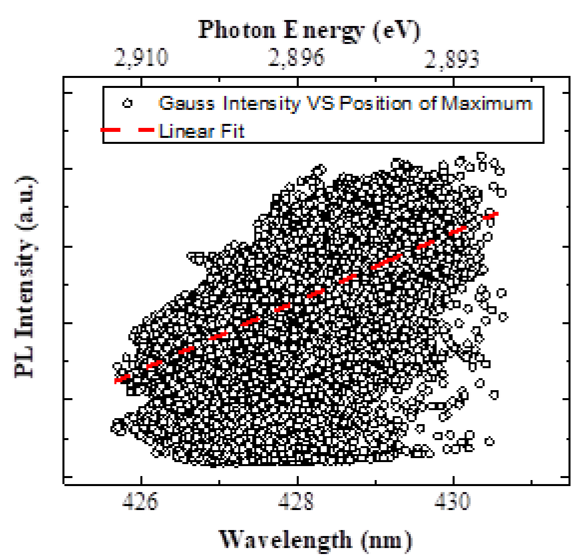

Fig. 10 Typical correlation graph between Gauss Intensity VS Position of Maximum (S2-1)

Correlation

The idea of correlation and its mathematical representation as a coefficient can be described as the joint variability of two random variables. The value of the coefficient can range between 1 and -1. If higher values of one variable corresponds to the higher values of the other, then it is positive and vice versa. In the present study higher PL intensity at longer wavelengths (lower photon energies) would correspond to positive values, whilst lower PL intensity would correspond to negative ones. Mathematically this is described by the following formula:

$$R = \frac{\sum(x_i - \bar{x})(y_i - \bar{y})}{\sqrt{\sum(x_i - \bar{x})^2 (y_i - \bar{y})^2}} \tag{4}$$

where R is the correlation coefficient, x_i with y_i are the values of *x* and *y* variables and $\bar{x}$ and $\bar{y}$ are the means of the *x* and *y* variable values.

A typical graphical representation is shown in Fig. 10. From first glance this looks like a chaotic datapoints set, however by using a simple linear fit, correlation can be extracted from the slope of the fitted formula (5). Using these values results of all the samples can be depicted graphically which could help look for some global tendencies.

$$y = a + bx \tag{5}$$

To grasp the idea of correlation visually, some areas of interest in Fig. 6 are marked with red circles, they represent areas in the sample, with which distinct cases can be demonstrated. Three main correlation types between PL intensity and peak position (or Gauss Center, when Gaussian function fit was used) were noticed in the study. For Fig. 6 b circles show that places emitting at longer wavelengths (or lower photon energies) have high PL intensity, which would correspond to positive correlation, as both of the variables here correspond to high values. In Fig. 6 c the complete opposite can be seen, that places with high PL signal emit shorter wavelengths (or higher photon energies), this means one variable has a high value whilst the other not, and this would be a sample with negative correlation. Finally, in Fig. 6 a it is almost impossible to decipher whether areas having high PL intensity correspond to longer or shorter wavelengths, so in this case it cannot be determined whether any correlation between these variables exist.

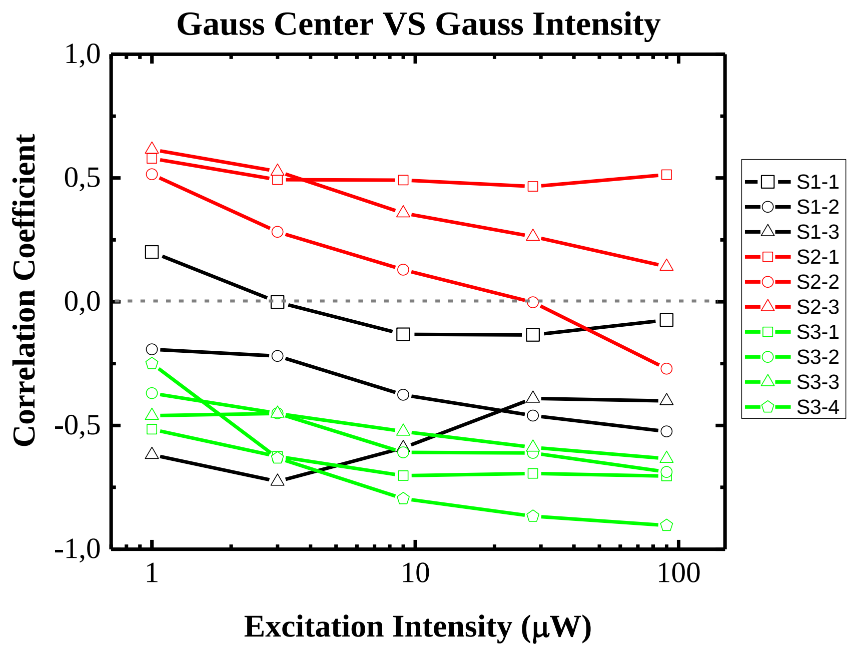

Fig. 11 Correlation coefficient (between Gauss Center and Gauss Intensity) dependance on excitation intensity of every C-plane sample from the study

Instead of manually comparing separate areas in images, point-by-point analysis was conducted to better characterize samples. Graphical representation of correlation coefficients for all of the samples is depicted in Fig. 11. Comparison between PL distributions and the calculated values was made to see if the results align with each other. Indeed, as was said for Fig. 6 b or sample S2-1 correlation should be positive and exactly that can be seen in the graph. Same for the negative correlation of sample S3-4 (Fig. 6 c) and S1-1 (Fig. 6 a) where there was no obvious correlation. From the graph it can also be seen that samples containing higher amounts of In tend to creep towards the negative values. Comparing these results with Fig. 7 it can be noticed that those same samples exhibit an overall lower PL intensity. The drop in efficiency is more noticeable when the emission wavelength is beyond the green part of the spectrum, hence this drop is called the "green gap" problem in InGaN LEDs, where the efficiency of the device drops substantially with increasing In content, which was noticed over 20 years ago [43]. Increasing the In content causes more biaxial strain between the GaN barrier and InN active region, which then increases the piezoelectric effect within the device and causes a stronger QCSE. This lowers the quantum efficiency of such devices. Even though InGaN LEDs are a mature field in the scientific community, this issue is still not fully understood.

To evaluate the approximate strength of the IEF within the c-plane samples modelling of PL band shift was performed under the assumption that it is predominantly caused by the screening of the built-in electric field. Some parameters such as carrier temperature and QW width were known beforehand and were entered into the program. Within the realistic ranges for each sample, other values such as conduction and valance band offset, electron and hole mass, dielectric constant and most importantly IEF were changed arbitrary for each calculation iteration, to get closer to the experimentally measured bandgap shift results and achieve a better fit. It was not possible to achieve high accuracy fits for all of the samples, however most of the samples achieved an acceptable similarity of experimental and theoretical values. The results of the modeling are shown in Fig. 12, within it, an inset of a typical fit can be seen. A clear tendency was noticed of decreasing IEF strength in samples emitting higher photon energies (or shorter wavelengths) thus having lower In. The highest IEF value was evaluated for sample of the highest indium content in the set. This is explained by the increased lattice mismatch between active and barrier layers within InGaN/GaN MQWs. The modeled results agree well with values found in literature [25],[44],[45].

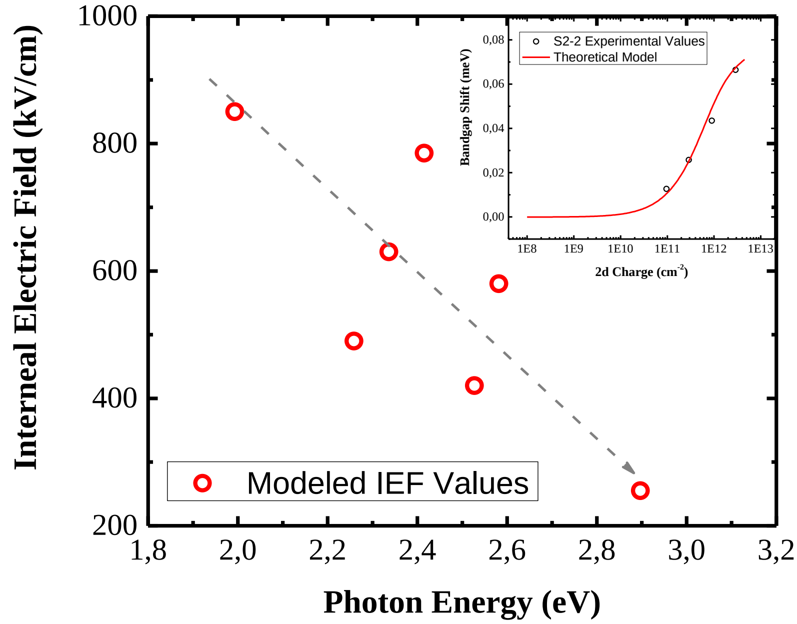

Fig. 12 Modeled IEF value dependence on emitted photon energies with a typical theoretical fit for the experimental values (top right corner)

There are a few models in the scientific community that are trying to explain observation of both positive and negative correlation. Carrier localization model could be used to explain observations in positive correlation samples. Samples with positive correlation usually have lower amount of indium (or larger amount of gallium), thus indium-rich regions are smaller (Fig. 13 a). As regions with higher indium have lower bandgap, carriers can be localized there, increasing their probability to recombine radiatively, hence boosting the luminescence signal and because carriers are confined in an area of lower bandgap, the emission is of lower energy photons. Thus, this localization lowers diffusion to NRCs. This model also is thought to be the main explanation behind high efficiency blue InGaN LED’s. [42]

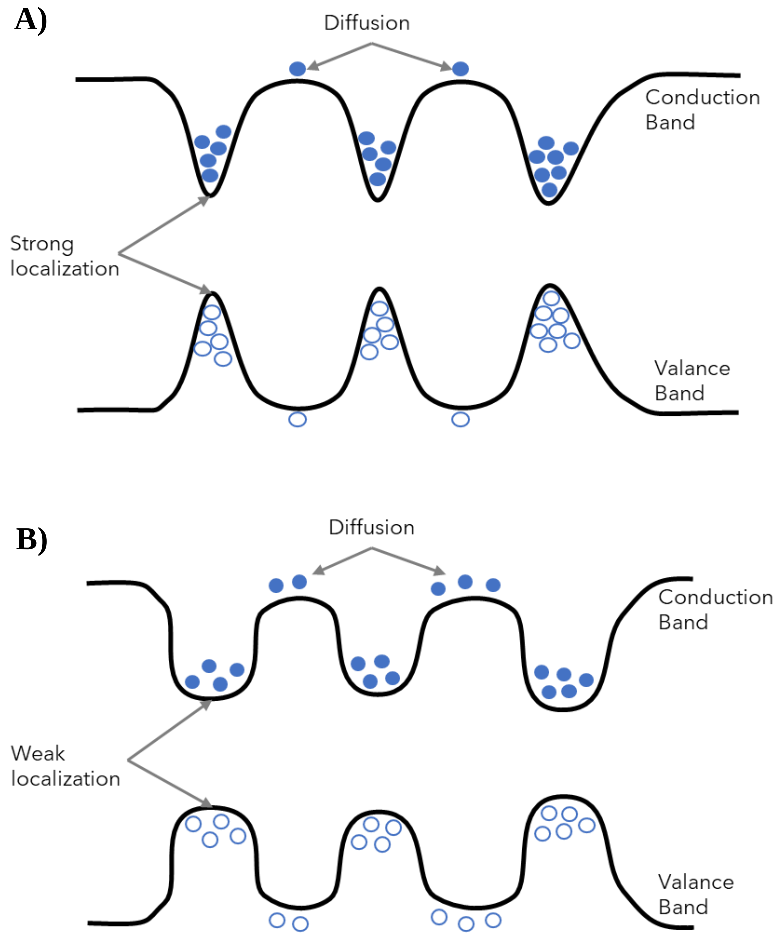

Fig. 13 Band diagrams of samples with a) low and b) higher indium amount

However, the same model cannot be used for negative correlation, which was noticed in samples with higher percentage of In. With more In those same In-rich places are now larger, it means that carriers can start to delocalize and diffusion to places such as NRCs, or other local minima becomes more probable. QCSE should also not be ignored as it tilts the energy bands which separates electron and hole from one another, thus decreasing radiative recombination [24] (as shown in Fig. 3 b). But in indium-rich areas the IEF is partially compensated due to an increased amount of photogenerated carriers. This tilts the band profile closer to a rectangular shape (as shown in Fig. 3 a) and shifts the band peak emission to larger photon energies (shorter wavelengths). This results in indium-rich areas to emit strong PL intensity at shorter wavelengths, which could explain the negative correlation results. [42]

The last thing to take away from the results of C-plane sets is the carrier dynamics with different excitation intensity. When taking a look back in Fig. 11 it can be noticed that by increasing the excitation intensity, coefficient values shift towards lower/negative values. One sample with an exception is S1-3. In Fig. 14 we can see its average PL spectrum and a second emission band is clearcly visible. It was towards the higher photon energies and this band skews the results and hence a discrepancy from the trend of all other samples can be seen. Nevertheless, the overall trend is clearly visible. At higher excitation intensities more and more localized carriers become delocalized. Delocalized carriers can reach defects where they recombine non-radiatively or they can be captured in other local minima of potential fluctuations and recombine radiatively. All this decreases the correlation strength between PL intensity and peak position as excitation intensity increases. For the samples that have negative correlation, it of course becomes even stronger. At higher excitation conditions, due to carriers in indium-rich areas, screening of the IEF takes place, this effectively increases the bandgap in those areas (blueshift of emission wavelength). With even higher intensities the IEF screening becomes even stronger and so the correlation becomes stronger (is moving towards value of -1).

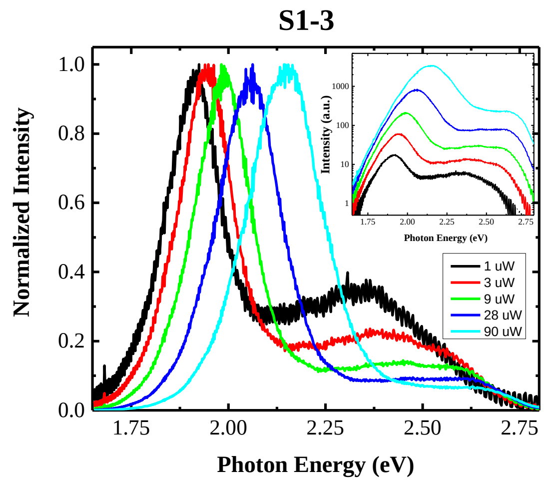

Fig. 14 Average PL spectrum of S1-3 sample with two visible emission bands

An extra observation that can be made is that the decrease in correlation seems to slow down with higher intensities. This could be tied to the increased densities of photogenerated nonequilibrium carriers. As their density increases, the IEF in the samples is compensated and the in-plane redistribution of the carriers does not change markedly.

M-plane Results

To expand upon our analysis about the IEF and its effects on PL intensity and peak wavelength correlation, a single m-plane sample set was also measured as theoretically it should be absent of the piezoelectric effect. First, spectral and statistical differences between the two growth orientations were analyzed. Fig. 15 depicts PL spatial distribution images of sample S4-2 at both medium (9 μW) excitation and maximum of 90 μW intensity. Images reveal similarities between the c-plane samples as both orientations have inhomogeneous In distributions, m-plane more so as the standard deviation of peak position of comparable wavelength c-plane samples, such as S1-1, S2-1 or S2-2 is around twice lower (on average), then for the m-plane samples, which could be attributed to the more challenging growth of m-plane samples. Furthermore, at an

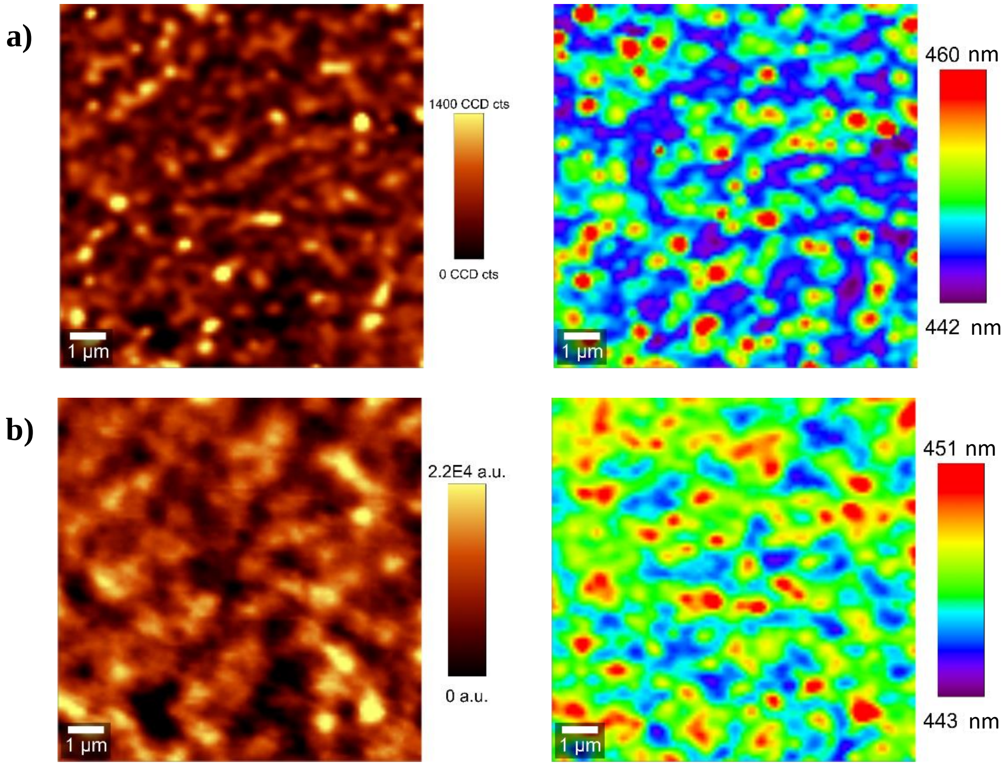

Fig. 15 Spatial distribution of spectrally integrated PL intensity and Gauss Center of sample S4-2 at a) 9 μW of excitation intensity and b) 90 μW of excitation intensity

excitation of 9 μW places emitting longer wavelengths have higher PL signal. When excitation is increased to around 90 μW these places become slightly more ambiguous, although generally it still seems that areas of higher PL signal emit photons of lower energy. The statistical results are depicted in Fig. 16. Average PL intensity graph depicts lower PL signal than for c-plane set, only one m-plane sample had similar intensity. Two of the samples with weakest luminescence were S4-5 and S4-6, which had thinner QWs compared to other m-plane samples. Huang *et al.* [46] have shown when samples are grown with relatively thin QWs, carrier delocalization is more likely because of the lack of structural uniformity, and those carriers are prone to nonradiative recombination. This along with more NRCs from higher indium incorporation could be the cause for less efficient PL. The second column of Fig. 16 where sample emission peak position is displayed, shows redshift of emission in areas of increased In within the active layer, similarly to c-plane sets. More surprising was the minor blueshift of emission wavelength for all m-plane samples, when excitation intensity increased. Although the shift does seem marginally smaller when compared with c-plane samples at similar emission wavelength, it is still present, which could be the first indications that these samples are not completely devoid of electric field, as they theoretically should be.

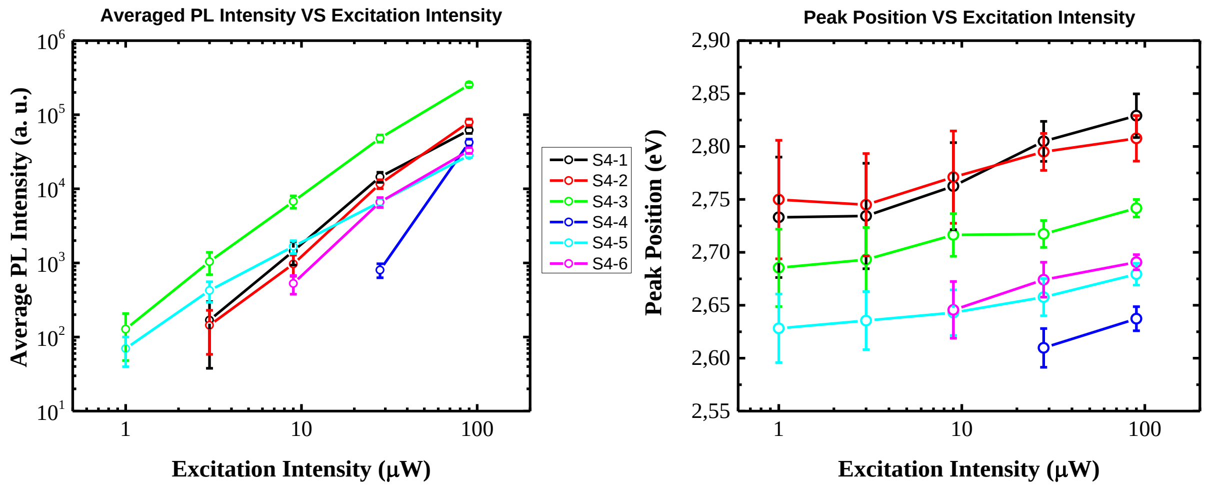

Fig. 16 Peak position and averaged PL intensity dependance on excitation intensity of the m-plane (4th) sample set [Error bars depict standard deviation for each value]

M-plane Set Correlation

Fig. 17 reveals the main correlation results for the m-plane sample set. PL intensity and peak position wavelength has positive correlation throughout the excitation intensity regimes. Thus, carrier localization model can be used to explain the achieved results. However, there might be some minor differences in the localized carriers between m-plane and c-plane samples. We concluded in a previous chapter that in c-plane positive correlation could be attributed to In-rich areas. C. J. Humphreys *et al.* [47] along with D. Watson-Parris *et al.* [48] reported the same conclusions, but on top of that by using effective mass approximation Watson-Parris calculated the potential energy landscape of the InGaN/GaN QWs. Their calculations showed that in the In-rich areas holes are strongly localized, whilst electrons due to the IEF were localized at the top of the QW interface. For the nonpolar InGaN/GaN MQWs S. Schulz *et al.* [49] made a prediction of an atomistic tight binding model which had a good agreement with the

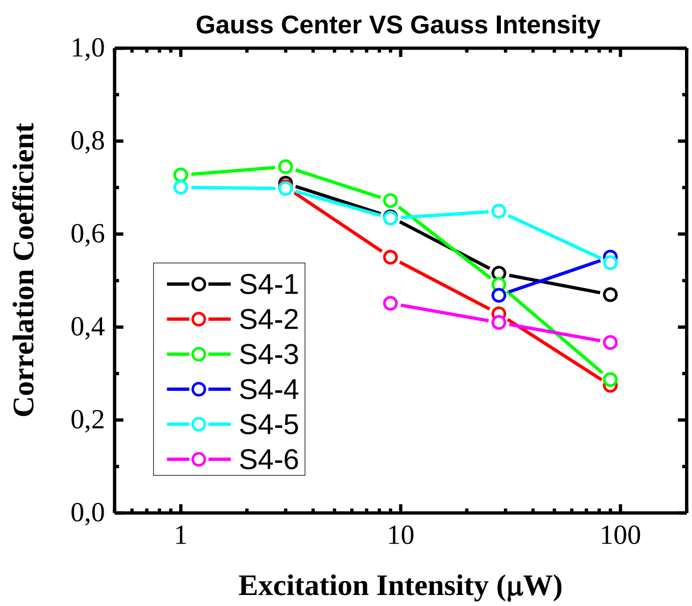

Fig. 17 Correlation coefficient (between Gauss Center and Gauss Intensity) dependance on excitation intensity of every M-plane sample

measured low temperature emission spectrum. In their prediction the hole localization stays the same however for the electrons, as there is no electric field, the Coulomb interaction between electrons and holes becomes predominant and both carriers become bound to each other, leading to localized excitons. This theory has also been supported by S. Marcinkevičius *et al.* [50] a decade ago.

When looking at the carrier dynamics with increasing excitation intensity it is visible that strong correlation is present at low to mid-level excitations. Only when high excitations are reached correlation strength decreases. This could be attributed to an electric field, however, if this is the case it is not from inside the material but rather as a consequence of the device structure as a *p-i-n* junction. Such structures inherently have an electric field. The MQW region is surrounded by an n-type and p-type layers, usually of GaN in InGaN LEDs. This could introduce the before mentioned slight blueshift of emission with increasing intensity, hence the correlation strength could start to slowly decrease as well. On the other hand, the blueshift might also be attributed to band filling effects. Both of these explanations could be used for the results as they have similar tendencies to the polar samples, unfortunately PL measurement methods alone cannot differentiate between these two effects.

Lastly to sum up the work, correlation coefficients between c-plane and m-plane samples have been compared. Its dependence on PL peak wavelength is depicted in Fig. 18. PL peak position was chosen as parameter for a qualitive representation of In content within the samples. As emission wavelength depends not only on the amount of In but such parameters as QW width, which in our study was not constant throughout the sets and could explain some of the outlier samples. The same explanation could be implemented for Fig. 12, when comparing the modeled IEF values. Nevertheless, the trend is still clearly visible for both figures. Another fact to mention, is that two of the m-plane samples are absent in Fig. 18 as it was not possible to achieve strong PL signal for measurements at an excitation of 3 μW. This once again might be tied to poor quality for those samples.

The results shown in Fig. 18 show a clear drop of correlation as PL peak wavelength increases for the c-plane samples. As the In content increases the IEF increases with it, due to increased lattice mismatch between InN and GaN. At smaller In content carrier localization model could explain positive correlation for c-plane samples, with the In-rich regions being smaller in comparison to GaN regions. Due to lower bandgap of InN, carriers can localize within such regions, increasing the probability of radiative recombination. On top of that IEF is comparatively low (Fig. 12) and so QCSE does not play a crucial role in such samples. However, further In incorporation means higher IEF strength which tilts the energy bands of the QW to a more triangle shape, separating holes and electrons, thus hindering radiative recombination. Furthermore, with In-rich regions becoming comparable in size with Ga-rich areas, carriers can start to delocalize and probability to reach NRCs or other local minima increases, further lowering PL intensity. Finally larger In-rich regions can accumulate higher carrier densities which may partially screen the IEF, this then tilts the energy bands back to a more rectangular shape, increasing the emitted photon energy, which means that those areas emit at shorter wavelengths but slightly higher intensity, reversing correlation sign from positive to negative. Such model could be used to explain the negative correlation behind high In content c-plane samples.

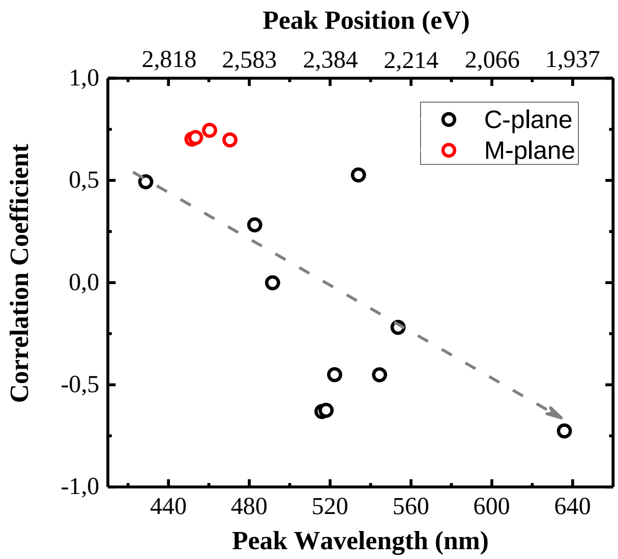

Fig. 18 Correlation coefficient (between Gauss Center and Gauss Intensity) dependance on peak wavelength/position for c-plane and m-plane sets at an excitation of 3μW

M-plane samples show a different trend of keeping a strong positive correlation. Although it must be said that the spectral range of m-plane samples is much narrower compared to c-plane, as it was not possible to acquire high-quality m-plane samples having higher amounts of In and emitting at longer wavelengths because of the difficulties in growth procedure. Even so, compared with c-plane samples having similar spectral characteristics, stronger positive correlation is observed. For these samples the carrier localization model explains well the observed results.

Conclusions

- Correlation coefficient between PL intensity and peak emission position of InGaN was studied using a confocal microscopy setup on sub-micrometer level. A large number of samples covering both a wide spectral range (~1.9 – 2.85 eV) along with c and m-plane growth orientation were investigated, allowing for a large data set to be analyzed and global tendencies for InGaN/GaN MQWs found.

- Correlation dependence on In amount in c-plane orientation samples was investigated with results showing a strong positive correlation at small In content (~ 12 %), with a constant decrease of correlation strength with increasing indium. At high In content (~ 25 %) correlation reached strong negative values.
- M-plane samples were investigated in a narrower spectral range (~ 2.6 – 2.85 eV) due to difficult growth at nonpolar orientations. Correlation showed even stronger positive values than for c-plane samples.
- Carrier localization model could be used to explain the positive correlation for both orientation samples as carriers can be localized at relatively small in size In-rich areas of lower bandgap in comparison with surrounding areas.
- Negative correlation observed in the highest In content c-plane samples could be due to the increased IEF as this increases the role of QCSE, which reduces radiative recombination probability rates by separating electrons and holes. Alongside this, the In-rich areas now become comparable to Ga-rich regions, which allows to accumulate higher density of carriers and partially screen IEF, tilting the band profile closer to a rectangular shape and enhancing local radiative recombination probability.

Santrauka

Baigiamojo darbo metu buvo siekiama išmatuoti koreliacijos koeficientą tarp fotoliuminescencijos (FL) intensyvumo ir FL juostos viršūnės bangos ilgio InGaN/GaN kvantinėse duobėse. Pasirinkti c-plokštumos bandiniai emituojantys visame regimosios šviesos spektre (~ 1.9 – 2.85 eV). Papildomai tirti bandiniai, užauginti ant m-plokštumos, norint patikrinti koreliacijos rezultatus be vidinio elektrinio lauko. M-plokštumos bandiniai emitavo siauresniame spektriniame intervale (~ 2.6 – 2.85 eV). Gauti m-plokštumos InGaN bandinius, turinčius didesnį nei ~15% indžio kiekį, vis dar yra sunku dėl sudėtingo auginimo. Visiems bandiniams užauginti buvo naudotas MOCVD metodas.

Norint gauti FL erdvinį pasiskirstymą buvo pasitelktas Alpha300 mikroskopas, dirbantis konfokaliniame režime. Bandiniai buvo žadinti 405 nm bangos ilgio lazeriniu diodu. Visiems bandiniams FL erdviniai pasiskirstymai buvo išmatuoti prie skirtingų FL žadinimo intensyvumų (1, 3, 9, 28, 90 μW). Rezultatų analizei buvo pasitelkta mikroskopo gamintojų pateikta programa, MATLAB, OriginLab ir programa įvertinti teorinį kvantinių duobių vidinį lauką, kurią sukūrė dr. V Liuolia.

Abiejų kristalinių orientacijų bandiniai parodė netolygų indžio pasiskirstymą. Didesnė indžio netvarka aptikta m-plokštumos bandiniuose, c-plokštumos bandiniuose. Tarpusavį lyginant c-plokštumos FL juostos maksimumo pozicijos ir FL intensyvumo paveikslus buvo pastebėta, jog bandiniuose turinčiuose mažiau indžio, intensyvios FL sritys emitavo ilgesnių bangos ilgių pusėję. Tai patvirtino stiprus teigiamas koreliacijos koeficientas. Bandiniuose su didesniu indžio kiekiu, buvo stebimi priešingi vaizdai. Aukštesnis FL intensyvumas buvo vietose, kurios švietė trumpesnius bangos ilgius. Koreliacijos koeficientas pakeitė ženklą ir pasiekė stiprią neigimą koreliaciją prie didžiausio indžio procento (~ 25 %). Atlikta statistinė duomenų analizė patvirtino iš paveikslų stebėtas tendencijas. M-plokštumos bandiniai turėjo pastovią ir dar stipresnę teigimą koreliaciją, palyginus su c-plokštumos. Teigimai koreliacijai paaiškinti tinka krūvininkų lokalizacijos modelis, kuriame krūvininkai yra lokalizuojami didesnio indžio kiekio srityse. Neigiama koreliacija, pastebėta didesnio indžio kiekio bandiniuose galėtu būti paaiškinama platėjančiomis indžio sankaupų sritimis, kuriose gali susikaupti didesnis krūvininkų kiekis dalinai ekranuojantis vidinį elektrinį lauką. Tokiu būdu kvantinės duobės profilis iš trikampio artėja link stačiakampio ir didina efektinį draustinį tarpą, bet kartu ir spindulinės rekombinacijos tikimybę dėl didėjančios elektrono ir skylės banginių funkcijų perklotos.

References

[1] S. Nakamura *et al.*, “P-GaN/N-InGaN/N-GaN Double-Heterostructure Blue-Light-Emitting Diodes,” *Jpn. J. Appl. Phys.*, vol. 32, no. Part 2, No.1A/B, pp. L8–L11, Jan. 1993, doi: 10.1143/JJAP.32.L8.

[2] Hiroshi Amano *et al.*, “P-Type Conduction in Mg-Doped GaN Treated with Low-Energy Electron Beam Irradiation (LEEBI),” *Jpn. J. Appl. Phys.*, vol. 28, pp. 2112–2114, 1989.

[3] “The 2014 Nobel Prize in Physics - Press release - NobelPrize.org.” https://www.nobelprize.org/prizes/physics/2014/press-release/ (accessed May 17, 2022).

[4] R. A. Arif *et al.*, “Type-II InGaN-GaNAs quantum wells for lasers applications Optical emission from ultrathin strained type-II InP/GaP quantum wells Appl,” *Cit. Appl. Phys. Lett.*, vol. 92, p. 2886, 2008, doi: 10.1063/1.2829600.

[5] D. V. P. McLaughlin *et al.*, “Progress in indium gallium nitride materials for solar photovoltaic energy conversion,” *Metall. Mater. Trans. A Phys. Metall. Mater. Sci.*, vol. 44, no. 4, pp. 1947–1954, Apr. 2013, doi: 10.1007/S11661-013-1622-1/FIGURES/1.

[6] A. Caria *et al.*, “Quantum efficiency of InGaN–GaN multi-quantum well solar cells: Experimental characterization and modeling,” *J. Appl. Phys.*, vol. 131, no. 22, p. 224501, Jun. 2022, doi: 10.1063/5.0076833.

[7] H. Zhang *et al.*, “InGaN-based nanowires development for energy harvesting and conversion applications,” *J. Appl. Phys.*, vol. 129, no. 12, p. 121103, Mar. 2021, doi: 10.1063/5.0035685.

[8] H. Dong *et al.*, “Improved carrier transport and photoelectric properties of InGaN/GaN multiple quantum wells with wider well and narrower barrier,” *Opt. Laser Technol.*, vol. 129, p. 106309, Sep. 2020, doi: 10.1016/j.optlastec.2020.106309.

[9] S. Nakamura *et al.*, *Introduction to nitride semiconductor blue lasers and light emitting diodes*. London ;;New York: Taylor & Francis, 2000.

[10] S. Ishimoto *et al.*, “Enhanced Device Performance of GaInN-Based Green Light-Emitting Diode with Sputtered AlN Buffer Layer,” *Appl. Sci. 2019, Vol. 9, Page 788*, vol. 9, no. 4, p. 788, Feb. 2019, doi: 10.3390/APP9040788.

[11] S. Nakamura, “The Roles of Structural Imperfections in InGaN-Based Blue Light-Emitting Diodes and Laser Diodes,” *Science (80-.).*, vol. 281, no. 5379, pp. 956–961, Aug. 1998, doi: 10.1126/SCIENCE.281.5379.956.

[12] R. A. Oliver *et al.*, “Microstructural origins of localization in {InGaN} quantum wells,” *J. Phys. D. Appl. Phys.*, vol. 43, no. 35, p. 354003, 2010, doi: 10.1088/0022-3727/43/35/354003.

[13] “De Broglie wavelength | IOPSpark.” https://spark.iop.org/de-broglie-wavelength (accessed May 22, 2022).

[14] S.-H. Baek *et al.*, “High-performance flat-type InGaN-based light-emitting diodes with local breakdown conductive channel,” *Sci. Reports 2019 91*, vol. 9, no. 1, pp. 1–7, Sep. 2019, doi: 10.1038/s41598-019-49727-4.

[15] C. Li *et al.*, “Effect of indium accumulation on the growth and properties of ultrathin In(Ga)N/GaN quantum wells,” *Mater. Des.*, vol. 190, p. 108565, May 2020, doi: 10.1016/j.matdes.2020.108565.

[16] D. Doppalapudi *et al.*, “Phase separation and ordering in InGaN alloys grown by molecular beam epitaxy,” *J. Appl. Phys.*, vol. 84, no. 3, p. 1389, Jul. 1998, doi: 10.1063/1.368251.

[17] H. N. Hussin *et al.*, “The effect of Multi Quantum Well growth regime transition on MQW/p-GaN structure and light emitting diode (LED) performance,” *Mater. Sci. Semicond. Process.*, vol. 121, Jan. 2021, doi: 10.1016/J.MSSP.2020.105431.

[18] R. Baddour-Hadjean *et al.*, “Reports on Progress in Physics Molecular beam epitaxy You may also like Mastering of Particle Size and Morphology of the Puckered Layer ’-V 2 O 5 Polymorph for Enhanced Na Electrochemical Properties Molecular beam epitaxy,” *Rep. Prog. Phys*, vol. 48, pp. 1637–1697, 1985.

[19] A. J. Ptak, “Principles of Molecular Beam Epitaxy,” *Handb. Cryst. Growth Thin Film. Ep. Second Ed.*, vol. 3, pp. 161–192, 2015, doi: 10.1016/B978-0-444-63304-0.00004-4.

[20] J. Huang, “Nitride semiconductor light-emitting diodes (LEDs) : materials, performance and applications,” 2014.

[21] E. L. Routh *et al.*, “Device quality templates of InxGa1-xN (x < 0.1) with defect densities comparable to GaN,” *Appl. Phys. Lett.*, vol. 117, no. 5, Aug. 2020, doi: 10.1063/5.0015419.

[22] H. Morkoç, “Handbook of Nitride Semiconductors and Devices: Electronic and Optical Processes in Nitrides,” *Handb.*

Nitride Semicond. Devices Electron. Opt. Process. Nitrides, vol. 2, pp. 1–846, Aug. 2009, doi: 10.1002/9783527628414.

[23] A. Senichev *et al.*, “Impact of growth conditions and strain on indium incorporation in non-polar m-plane (10 1 ¯ 0) InGaN grown by plasma-assisted molecular beam epitaxy,” *APLM*, vol. 7, no. 12, p. 121109, Dec. 2019, doi: 10.1063/1.5121445.

[24] J. Mo *et al.*, “Dynamic piezo-phototronic effect in InGaN/GaN multiple quantum wells,” *Superlattices Microstruct.*, vol. 155, Jul. 2021, doi: 10.1016/J.SPMI.2021.106926.

[25] C. K. Huang *et al.*, “Measurement of internal electrical field across InGaN quantum wells in GaN LEDs,” *Mater. Chem. Phys.*, vol. 265, Jun. 2021, doi: 10.1016/J.MATCHEMPHYS.2021.124514.

[26] S.-C. Tsai *et al.*, “Piezoelectric effect on compensation of the quantum-confined Stark effect in InGaN/GaN multiple quantum wells based green light-emitting diodes,” 2016, doi: 10.1016/j.nanoen.2016.08.061.

[27] H. Y. Ryu *et al.*, “A comparative study of efficiency droop and internal electric field for InGaN blue lighting-emitting diodes on silicon and sapphire substrates,” *Sci. Rep.*, vol. 7, Apr. 2017, doi: 10.1038/SREP44814.

[28] P. Waltereit *et al.*, “Nitride semiconductors free of electrostatic fields for efficient white light-emitting diodes,” *Nature*, vol. 406, no. 6798, pp. 865–869, Aug. 2000, Accessed: Nov. 12, 2022. [Online]. Available: https://go.gale.com/ps/i.do?p=AONE&sw=w&issn=00280836&v=2.1&it=r&id=GALE%7CA188081024&sid=googleScholar&linkaccess=fulltext.

[29] K. M. Kelchner *et al.*, “GaN Laser Diodes on Nonpolar and Semipolar Planes,” *Semicond. Semimetals*, vol. 86, pp. 149–182, 2012, doi: 10.1016/B978-0-12-391066-0.00004-6.

[30] M. Sawicka *et al.*, “Indium incorporation in semipolar ($20\bar{2}1$) and nonpolar ($10\bar{1}0$) InGaN grown by plasma assisted molecular beam epitaxy,” *J. Cryst. Growth*, vol. 459, pp. 129–134, Feb. 2017, doi: 10.1016/J.JCRYSGRO.2016.11.105.

[31] Y. Cao *et al.*, “Photoluminescence study of non-polar m-plane InGaN and nearly strain-balanced InGaN/AlGaN superlattices,” *J. Appl. Phys.*, vol. 127, no. 18, p. 185702, May 2020, doi: 10.1063/5.0003740.

[32] D. Sutherland *et al.*, “Optical studies of non-polar m-plane () InGaN/GaN multi-quantum wells grown on freestanding bulk GaN,” *Phys. status solidi*, vol. 252, no. 5, pp. 965–970, May 2015, doi: 10.1002/PSSB.201451563.

[33] P. Dawson *et al.*, “The nature of carrier localisation in polar and nonpolar InGaN/GaN quantum wells ARTICLES YOU MAY BE INTERESTED IN,” *J. Appl. Phys*, vol. 119, p. 181505, 2016, doi: 10.1063/1.4948237.

[34] M. Minsky, “Microscopy apparatus,” US3013467A, 1957.

[35] V. E. lbbe and ao Professor in Jena, “Beiträge zur Theorie des Mikroskops und der mikroskopischen Wahrnehmung,” *Arch. für Mikroskopische Anat. 1873 91*, vol. 9, no. 1, pp. 413–468, Dec. 1873, doi: 10.1007/BF02956173.

[36] F. L. Pedrotti *et al.*, *Introduction to Optics*. Cambridge University Press, 2017.

[37] J. Mickevičius *et al.*, “Photoluminescence dynamics of AlGaN quantum wells with built-in electric fields and localized states,” *Phys. status solidi*, vol. 207, no. 2, pp. 423–427, Feb. 2010, doi: 10.1002/PSSA.200925227.

[38] X. Wang *et al.*, “Influence of in doping in GaN barriers on luminescence properties of InGaN/GaN multiple quantum well LEDs,” *Superlattices Microstruct.*, vol. 114, pp. 32–36, Feb. 2018, doi: 10.1016/j.spmi.2017.11.038.

[39] N. M. Shmidt *et al.*, “The impact of the surface morphology on optical features of the green emitting InGaN/GaN multiple quantum wells,” *J. Cryst. Growth*, vol. 520, pp. 82–84, Aug. 2019, doi: 10.1016/j.jcrysgro.2019.05.015.

[40] Takahiro Numai, “Fundamentals of Semiconductor Lasers,” *Fundam. Semicond. Lasers*, vol. 93, 2004, doi: 10.1007/B97531.

[41] J. Mickevičius *et al.*, “Spatial redistribution of photoexcited carriers in InGaN/GaN structures emitting in a wide spectral range,” *J. Lumin.*, vol. 199, pp. 379–383, Jul. 2018, doi: 10.1016/J.JLUMIN.2018.03.078.

[42] K. Okamoto *et al.*, “Confocal microphotoluminescence of InGaN-based light-emitting diodes,” *J. Appl. Phys.*, vol. 98, no. 6, p. 064503, Sep. 2005, doi: 10.1063/1.2037869.

[43] L.-H. Peng *et al.*, “Piezoelectric effects in the optical properties of strained InGaN quantum wells,” 1999.

[44] L. Guo *et al.*, “The influence of internal electric fields on the transition energy of InGaN/gaN quantum well,” *J. Cryst. Growth*, vol. 298, no. SPEC. ISS, pp. 522–526, Jan. 2007, doi: 10.1016/J.JCRYSGRO.2006.11.078.

[45] X. Hou *et al.*, “Optical properties of InGaN-based redmultiple quantum wells,” *Appl. Phys. Lett*, vol. 120, p. 261102, 2022, doi: 10.1063/5.0096155.

[46] X. Huang *et al.*, “Anomalous carrier dynamics and localization effects in nonpolar m-plane InGaN/GaN quantum wells at high temperatures,” *Nano Energy*, vol. 76, p. 105013, Oct. 2020, doi: 10.1016/J.NANOEN.2020.105013.

[47] C. J. Humphreys *et al.*, “The atomic structure of polar and non-polar InGaN quantum wells and the green gap problem,” *Ultramicroscopy*, vol. 176, pp. 93–98, May 2017, doi: 10.1016/J.ULTRAMIC.2017.01.019.

[48] D. Watson-Parris *et al.*, “Carrier localization mechanisms in In x Ga 1−x N/GaN quantum wells,” *Phys. Rev. B*, vol. 83, no. 7, pp. 115321–115322, 2011, doi: 10.1103/PhysRevB.83.115321.

[49] S. Schulz *et al.*, “Structural, electronic, and optical properties of m-plane InGaN/GaN quantum wells: Insights from experiment and atomistic theory,” *Phys. Rev. B*, vol. 92, p. 235419, 2015, doi: 10.1103/PhysRevB.92.235419.

[50] S. Marcinkevičius *et al.*, “Photoexcited carrier recombination in wide m-plane InGaN/GaN quantum wells,” *Appl. Phys. Lett*, vol. 103, p. 111107, 2013, doi: 10.1063/1.4820839.